SPACE SCIENCE AND ENGINEERING CENTER
University of Wisconsin-Madison

The Schwerdtfeger Library
1225 W. Dayton Street
Madison, WI 53706

23 July 2009

Attn: William Emanuel
NASA Headquarters, Code YS
Washington, DC 20546

RE: Award NNG04GJ46G Final Report

Dear Mr. Emanuel:

Attached for your records is a copy of the final summary of research, as required the above listed grant terms. We apologize for the lateness of the submission.

If you have any questions or need further information, please contact PI Robert Knuteson with technical questions at (608) 263-7974 or myself for all other issues at (608) 262-0985. Thank you for your cooperation and continued support.

Sincerely,

John P. Roberts
Associate Director
SSEC

Cc: 144-MT27
B. Knuteson
4669
Grants Officer
CASI
ONR Chicago

I:/jennys/4669Final.doc

Land Surface Characterization Using High Spectral Resolution AIRS and Moderate Spatial Resolution MODIS Observations from the EOS Aqua Platform

A Final Report to

The National Aeronautics and Space Administration
Office of Research and Applications for
NASA grant NNG04GJ46G

For the Period
15 April 2006 to 15 April 2008

Submitted by the

Cooperative Institute for Meteorological Satellite Studies
Space Science and Engineering Center (SSEC)
at the University of Wisconsin-Madison
1225 West Dayton Street
Madison, Wisconsin 53706
(608) 262-0544

Principal Investigator
Robert O. Knuteson

Co-Investigators:
Steven A. Ackerman
Henry E. Revercomb
David C. Tobin
Brian J. Osborne

April 2008

Table of Contents

Land Surface Characterization Using High Spectral Resolution AIRS and Moderate Spatial Resolution MODIS Observations from the EOS Aqua Platform

1. *Introduction*

This is the final report of NASA grant NNG04GJ46G titled "Land Surface Characterization Using High Spectral Resolution AIRS and Moderate Spatial Resolution MODIS Observations from the EOS Aqua Platform" submitted by the University of Wisconsin-Madison Space Science and Engineering Center Cooperative Institute for Meteorological Satellite Studies.

The new science contributed by this report is made possible because of the important new spectral observations provided by the AIRS instrument on the Aqua platform. The Aqua launch in May 2002 opened a new era in meteorological satellite observations that will be continued for at least the next 30 years. Table 1 places the Aqua launch into the perspective of the long-term climate record from satellites. The EOS Aqua satellite observations are building upon the climate record of the current NOAA TIROS satellite series. These meteorological observations are designed to improve the predictive capabilities of global numerical weather prediction (NWP) models (Susskind et al. 1984; Chedin et al. 1985; Smith 1989). This report addresses one of the longstanding problems in the interpretation of infrared data from the operational meteorological satellites, i.e., the accurate retrieval of land surface temperature from satellite infrared observations. With the significant increase in the number of infrared spectral channels (2378 channels for AIRS compared with 30 for HIRS), comes an increase in land surface emissivity information. The physics of infrared remote sensing is such that the spectral channels that sense the lower troposphere also receive a significant contribution from emission from the surface. Unless the spectral and spatial variation of land surface emissivity is taken into account (either in the profile retrieval or the NWP data assimilation) absolute errors can be introduced into the derived atmospheric thermodynamic structure. This project addresses the need in the EOS program for high spectral resolution land surface emissivity for atmospheric remote sensing.

The future of the U.S. meteorological satellite program falls under the Integrated Program Office (IPO) NPOESS program (Nelson and Cunningham 2002). The NPOESS program has identified the Visible Infrared Imaging Radiometer Suite (VIIRS) and the Cross-track Infrared Sounder (CrIS) as a follow-on to the EOS MODIS and AIRS sensors. Since the NPOESS platform will not be ready for launch until 2013 at the earliest, the NPOESS Preparatory Project (NPP) will be launched to cover the gap between the EOS and NPOESS platforms (Murphy et al. 1998). Meanwhile, Europe's new EPS program is providing the afternoon meteorological satellite platform with the launch of METOP in 2007 (Diebel et al. 1997). Given this roadmap to the future, the exploitation of the high spectral resolution AIRS and the high spatial resolution MODIS data on the EOS Aqua platform is an investment with near-term benefits in weather prediction but long term benefits to the climate record.

Table 1. Meteorological satellites; past, present, and future.

Series	Start	End	Imager	IR Sounder
NOAA POES TIROS	1978	2009+	AVHRR	HIRS
NASA EOS AQUA	2002	2009	MODIS	AIRS
EUMESAT EPS METOP	2005	2019+	AVHRR	HIRS, IASI
NASA/IPO NPP	2010	2015+	VIIRS	CrIS
IPO NPOESS	2013	2029+	VIIRS	CrIS

2. *Objectives and Significance*

The first project objective is a better utilization of satellite sounding data over land. The Coordination Group for Meteorological Satellites (CGMS), an international body wherein NOAA and NASA participate, has identified a need for work on this goal; they noted in their report "the use of satellite radiances over land needs further attention, as there is a growing need for improved use of satellite data in some land areas of the globe; surface emissivity effects must be accommodated to achieve positive results". [Report on CGMS XXVI held 6 – 10 July 1998 in Nikko, Japan. EUMETSAT publication.] In general, the current NWP data assimilation system uses radiosondes and not satellite data over land and satellite data with a few ship based observations over oceans – this creates false gradients that hinder better weather forecasts (Derber and Wu, 1998; Schmidt et al., 2002). Some NWP centers are starting to use satellite radiances not influenced by the surface (channels in H_2O and CO_2 absorption bands). Forward model calculated radiances are critical to the radiance assimilation process, which implies that characterization of the surface emissivity and temperature is necessary. The new high spectral resolution infrared data has the information content to estimate both surface skin temperature and emisssivity. The NASA AIRS team algorithm is designed to provide a simultaneous retrieval of atmospheric profiles, land-surface temperature, and surface emissivity (Chahine et al., 1999). Evaluation of the quality of the retrieved land surface products from AIRS is one of the main proposed activities of this project. The investigators have demonstrated a new technique for the simultaneous separation of land surface temperature and emissivity that takes advantage of the high spectral resolution information contained in the AIRS observations (Knuteson et al., 2004). This report will apply the investigator technique for land surface temperature and emissivity retrieval to AIRS data in a quality assessment of the operational AIRS product. Simultaneous land surface and atmospheric profile retrievals have also been obtained from MODIS data (Ma et al., 2000, 2002). Li used a classification scheme to characterize cloud and surface properties in radiance space in order to retrieve atmospheric information at the 1 km MODIS resolution (Li et al., 2003). The comparison of results from AIRS and MODIS operational and research products for different ecosystems will be an important contribution of this project.

The second project objective is the study of the evolution of land surface characteristics. The accuracy of the land surface temperature derived from satellite infrared observations is dependent on accurate knowledge of the land surface emissivity. Surface emissivity errors of 1.5 % lead to surface temperature errors of about 1 °C (Korb et al., 1996). One of the objectives of this report is the quantification of the temporal, spatial, and spectral variation of surface emission that is caused by natural and human-

induced change in the land cover distribution in marginal zones surrounding desert regions. These marginal zones are important for the livelihood of millions of people around the world. They are also the regions where poor land use practices, e.g. overgrazing, can cause a degradation of the plant ecosystems leading to the potential for desertification (Balba 1980). Land use practices that cause change in land cover can induce biophysical feedback on the climate system by increasing the area of exposed bare soil with subsequent changes in land surface thermal emission. This project will contributes to understanding these forcing mechanisms by providing a quantifiable estimate of the land surface thermal emission as parameterized by an effective surface temperature and infrared surface emissivity to complement other estimates of land cover and land use. This study presents time series of surface temperatures and emissivities to characterize the natural variability of surface emission.

3. *Background*

Ground-based Measurements

The investigators began intensive research into the characteristics of infrared land surface emission while analyzing the upwelling radiance observations from the UW High-resolution Interferometer Sounder (HIS) onboard the NASA high altitude ER-2 aircraft (Xie 1994). Flights were conducted over the Department of Energy (DOE) Atmospheric Radiation Measurement (ARM) Southern Great Plains (SGP) central facility in north central Oklahoma (Stokes and Schwartz 1994). Considerable spectral variability was observed in the infrared window region as the aircraft passed over an agricultural region of mixed scene types. These observations led, in 1997, to the first UW-CIMSS ground-based measurements of pure scene types in the vicinity of the DOE ARM SGP central facility site. These observations were made using the UW research vehicle ("AERIBAGO") and an angle scanning version of the UW Atmospheric Emitted Radiance Interferometer (AERI) (Knuteson 2001b).

A sample of the soil characteristic of the SGP central facility region was collected by the UW at that time and sent to Dr. Wan of UCSB for laboratory analysis. Those laboratory measurements can be found in the MODIS UCSB Emissivity Library labeled "Oklahoma Soil". These in situ measurements build upon and are consistent with the breadth of research into terrestrial materials that already exist in the literature (Salisbury and D'Aria 1992, 1994; Korb et al. 1994; Wan and Dozier 1997).

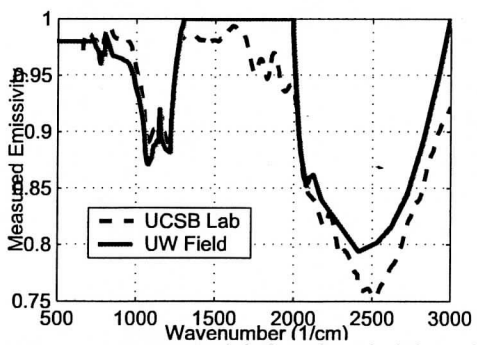

Figure 1. Measured infrared emissivity of bare soil from the DOE ARM SGP central facility collected in 1997 by UW personnel.

Figure 1 shows one of the UCSB laboratory measurements of the Oklahoma soil (#10) after sample preparation compared with in-the-field observations of the bare soil made "in situ" with the UW AERIBAGO. The differences between the two curves can be largely attributed to preparation of the soil sample for laboratory analysis. No UW field measurements were made in the 5 to 7 micron region because of the strong contamination of water vapor in the free atmosphere.

The remote sensing of land surface temperature (LST) from satellite requires a detailed knowledge of infrared land surface emissivity (Dozier and Wan 1994). Roughly speaking, a 2% error in the knowledge of the land surface emissivity near 10 microns leads to an error in the derived surface temperature of about 1 Kelvin. Since the emissivity of bare soil can vary across the infrared spectrum by 10% or more, errors in the remote sensing of surface temperature from satellites can be substantial. In order to improve our knowledge of the spectral dependence of the infrared land surface emissivity (LSE) in the vicinity of the ARM SGP central facility, the UW-CIMSS developed a model of the LSE across the infrared window regions, from 3.3 to 14 μm, at high spectral resolution (Tobin et al. 2003; Knuteson et al. 2004). The best estimate LSE model for the SGP site was created in April 2001 based upon three key elements; (1) UW on-site ground surveys of land cover and land use, (2) UW ground-based surface emissivity measurements, and (3) UW aircraft-based surface emissivity measurements.

The land cover of the region containing the ARM SGP central facility is dominated by agricultural land use. The local landowners balance cattle ranching with the cultivation of wheat and other grain crops. This land use combines with the relatively small quarter-mile to half-mile square dimensions of farm fields to produce a very heterogeneous land cover distribution. In an attempt to understand and characterize the land cover distribution, the UW conducted in situ ground surveys in November 2000, March 2001, June 2002, and November 2002 (Osborne et al. 2003). Figure 2 shows the survey region, a nine mile (15 km) square grid including the ARM central facility. Visual observations of vegetation cover and land type were used to generate distributions according to land use classifications. The comparison of the June 2002 survey to the 1992 US Geological Survey (USGS) database of this region is also shown in Figure 2. Several important generalizations were drawn from these site surveys. First, the two dominant land cover types in this region are pasture and grains (25% and 64% respectively in June 2002). The cattle ranchers maintain pasture lands that are multi-year grasslands. Since grassland covers the underlying soil (when not subject to overgrazing), the grassland areas are effectively 100% vegetated all year round. In contrast, the grain production is dominated by winter wheat cultivation. Winter wheat is planted in the autumn (September-November), rapidly grows to a height of 3 to 6 inches but goes dormant over winter (December-March) and continues growth in the spring (April-May) ending up with a harvest in mid summer (June-August) at which point the cycle repeats.

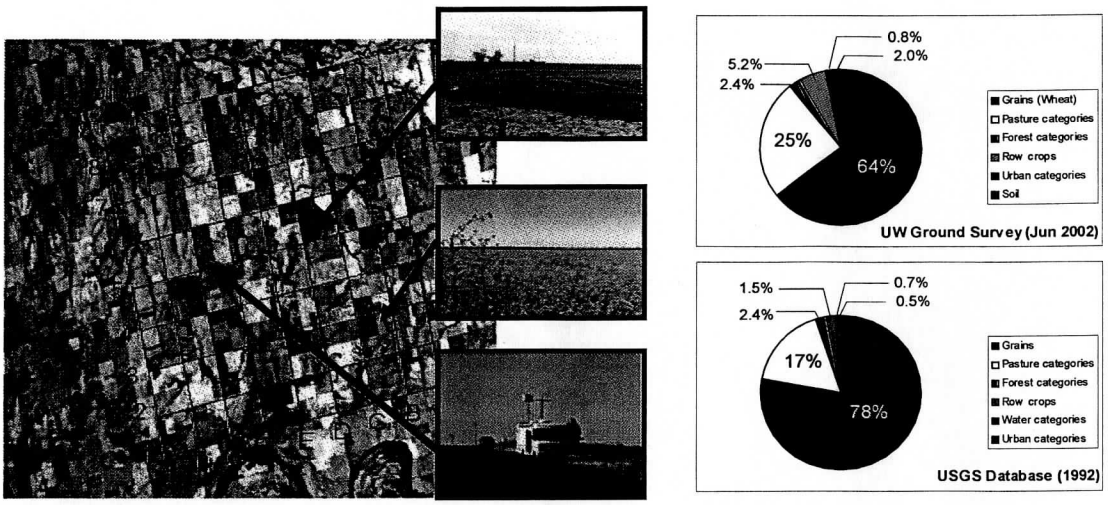

Figure 2. On-site surveys have been conducted by UW-SSEC personnel in order to characterize the distribution of land cover in vicinity of the ARM SGP central facility near Billings, Oklahoma. The survey grid is superimposed on a MODIS Airborne Simulator image from 31 March 2001 (North is down on the image). The June 2002 survey results are compared to the 1992 USGS database. Pasture land and wheat fields are the two dominant land cover types.

Aircraft-based Measurements

High altitude aircraft observations have been used to estimate the spatially averaged land surface emissivity over a 15-km region centered at the SGP ARM central facility. The 15-km spatial domain is chosen to match the satellite sub-pixel footprint of the NASA AIRS instrument on the EOS Aqua platform. Aircraft observations from the UW Scanning High-resolution Interferometer Sounder (similar to the ground-based AERI instrument) as well as observations from the NASA NPOESS Atmospheric Sounder Testbed – Interferometer (NAST-I) have been collected over several field campaigns (Revercomb et al. 1998, 2003). A complete analysis of one of these observation cases can be found in Knuteson et al., 2004. Figure 3 shows the result of fitting the UW LSE model pure emissivity scene types to a spatially averaged emissivity obtained from aircraft observations over the ARM SGP site during the TX-2001 experiment in March 2001 (Moeller et al. 2001). Similar results were obtained during the AFWEX experiment in November 2000 from both the Scanning HIS and the NAST-I (Tobin et al. 2002)

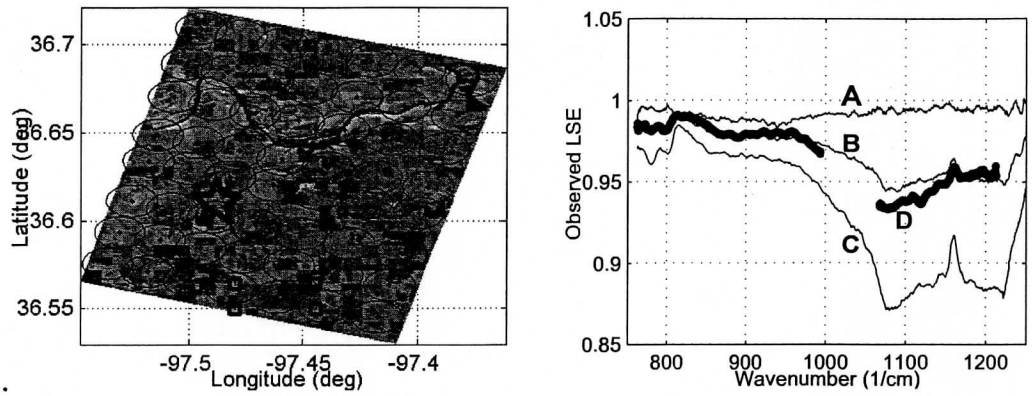

Figure 3. Land surface emissivity derived from aircraft observations of upwelling radiance from the UW Scanning HIS interferometer averaged over a 15-km region in the vicinity of the ARM SGP central facility. The observations were collected from the NASA high altitude ER-2 aircraft on 31 March 2001 during the Terra Experiment-2001 (TX-2001). The "best fit" effective LSE, labeled "D", is compared in the right-hand panel to a linear combination of pure scene types: 100% vegetation ("A"), 60% vegetation/40% bare soil ("B"), and 100% bare soil ("C").

An algorithm developed by UW-CIMSS for the separation of surface temperature and surface emissivity using high spectral resolution was demonstrated with high altitude aircraft observations and applied in this study to AIRS satellite radiances (Knuteson et al. 2004). The theoretical basis for the separation of surface temperature and emissivity using high spectral resolution satellite observations is presented in Knuteson et al. 2004.

4. *AIRS Version 5 Validation*

4.1 Overview

This report will first provide examples at validation sites to illustrate two different surface types; the Egypt One site in the Libyan Desert and the DOE ARM Southern Great Plains site in an agricultural region. A global comparison of AIRS and MODIS products is then presented that helps to characterize the uncertainties in these products by land type. All the data products identified for use in this project are either available through the Goddard DAAC or were derived directly by the investigator from radiances obtained from the DAAC.

4.2 Egypt One Site

A case study is provided for two granules (6 minutes each) of top of the atmosphere radiance observations from the NASA AIRS spectrometer on the EOS Aqua platform. The observations are from a night-time (00:00-00:06 UTC) and a daytime (11:00-11:06 UTC) overpass of the Libyan Desert in North Africa on 16 November 2002. The area

over Egypt and the Red Sea is largely cloud-free as can be seen in the coincident daytime visible imagery from the MODIS sensor shown in Figure 4. Skin temperature estimates from the European Center for Medium-range Weather Forecasting (ECMWF) at the time of the daytime overpass are shown in Figure 5 along with the AIRS brightness temperature from a narrow microwindow at about 12 μm. A square symbol in Figure 5 marks the location of a fairly uniform region of the Libyan desert used for satellite validation referred to as "Egypt One" (27.12 N, 26.10 E). A desert site was chosen to illustrate the infrared spectral signature of silicate minerals (coarse sand) that is present in the high spectral resolution AIRS observations. Laboratory and ground-based observations of coarse sand suggest that a large emissivity contrast is expected between 12 μm and 4 μm and also between 12 μm and 9 μm as shown in Figure 6.

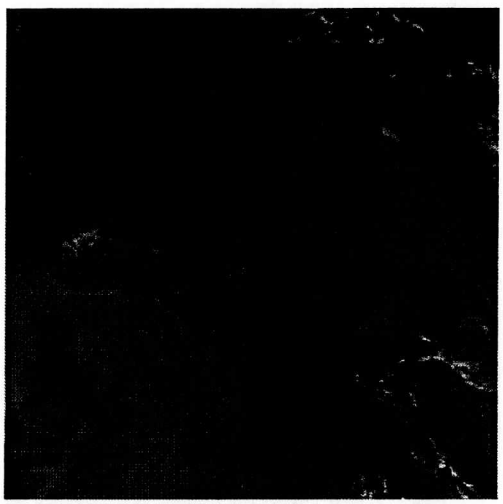

Figure 4. MODIS color composite image of the Libyan desert and the Red Sea from an Aqua overpass at 11:00-11:06 UTC on 16 November 2002. Most of the region of interest is cloud-free with the notable exception of an area of low cloud in the Mediterranean extending over the North African coastal plain.

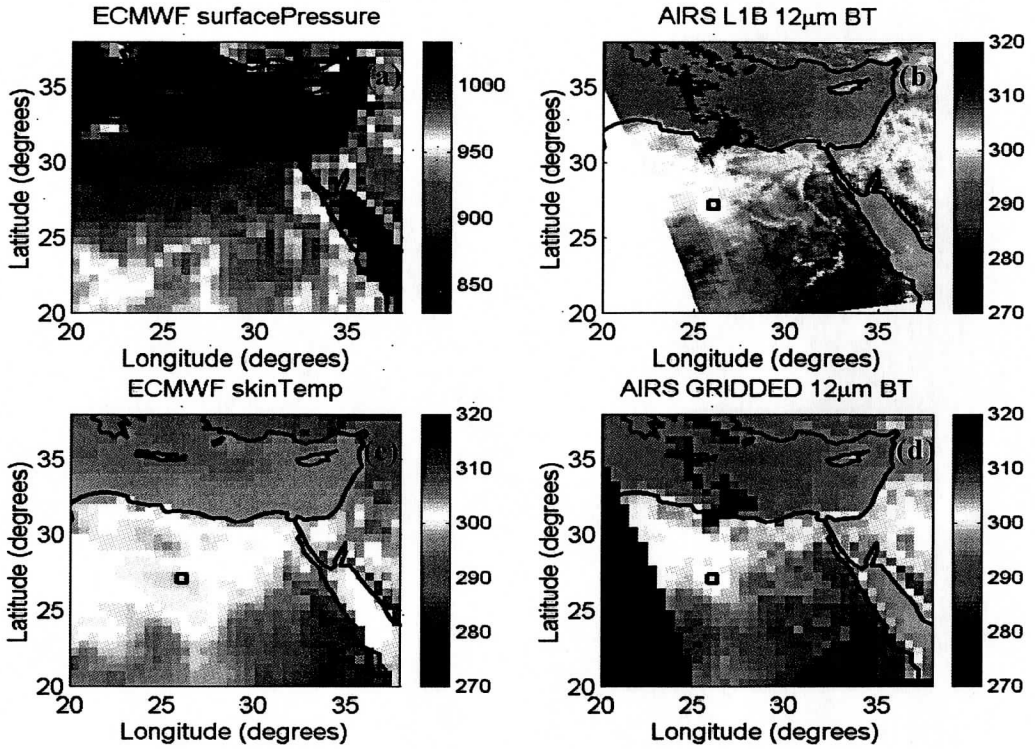

Figure 5. ECMWF (a) surface pressure (elevation) map and (c) analysis skin temperature for the 12 UTC analysis compared to AIRS observations of (b) 12 μm brightness temperature (830-832 cm-1) at nominal 15-km resolution and (d) gridded to match the ECMWF 0.5 degree spatial resolution for an NASA Aqua overpass at 11:00-11:06 UTC on 16 November 2002. The square symbol marks the "Egypt One" satellite validation site (27.12 N, 26.10 E). The AIRS L1B 12 μm brightness temperature is fairly uniform at the location of the Egypt One site. The ECMWF model suggests that cool, moist air in the atmospheric boundary layer has pushed down from the Mediterranean Sea in the north, thereby suppressing the daytime surface skin temperatures over the Libyan Desert.

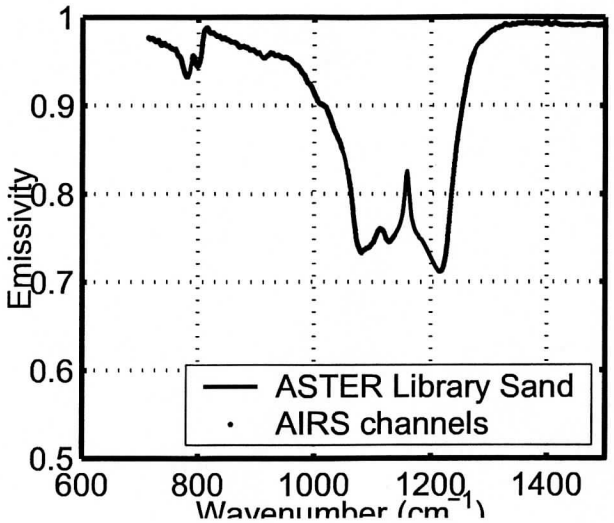

Figure 6. The spectral emissivity for alluvial sand (FGG027c) obtained from the JPL ASTER spectral library (left) used for comparison to observations from the NASA Aqua satellite over the Egypt One validation site(right). The AIRS channels are marked in red.

To estimate the size of the IR surface reflection term, a calculation has been performed using the Line-By-Line Radiative Transfer Model (LBLRTM) and the HITRAN database with the ECWMF analysis of the temperature and water vapor profile over the Egypt One site. The result of this calculation is shown in Fig. 7 under two assumptions of surface reflectivity; a constant emissivity of 0.98 at all wavelengths and the more realistic laboratory quartz sand emissivity spectrum shown in Fig. 6. The results are compared against the nominal AIRS noise level in each channel. Note the change of scale between the 2% reflectivity case and the more realistic laboratory estimate. A constant value of 0.98 has been commonly used in Numerical Weather Prediction at ECMWF for all land surfaces. Figure 7 illustrates that the AIRS sensor has the sensitivity and spectral coverage that requires an improved characterization of the land surface emissivity spectrum if this data is to be effectively used over land. Errors in surface emissivity have been shown to lead to errors in the retrieval of boundary layer water vapor from the sounder observations. However, the sensitivity of the AIRS instrument suggests that it should be possible to derive the infrared surface emissivity signature from the AIRS data directly. The following illustrates a method for deriving the land surface emissivity from individual clear AIRS fields of view with the goal of improving both land surface temperature estimates and the accuracy of water vapor profile retrievals.

The brightness temperature contrast between 12 μm (830-832 cm^{-1}) and 9 μm (1092-1099 cm^{-1}) is shown in Fig. 8 both as spatial maps and as brightness temperature histograms for the daytime AIRS observations. Note that both the ocean and vegetation regions (Nile river and coastal zone) have a 9 minus 12 μm brightness temperature difference close to zero while the exposed sand and rocks in the Libyan desert show brightness temperature differences up to 20 degrees. This is due to the fact that the

infrared emissivity of both vegetation and water have relatively little spectral contrast across the 8 to 12 μm infrared window compared to the spectral signatures of exposed minerals. In particular, the fractional coverage of vegetation in the AIRS instrument field of view determines the magnitude of the observed spectral contrast, with higher vegetation fractions leading to reduced spectral contrast. The 4 μm brightness temperature variation is not shown for the daytime case due to contamination of the Earth emitted radiance by solar reflection at these wavelengths. An analysis of the 4 μm surface emissivity for the night-time case is given in the results section below. The AIRS infrared spectrum closest to the the Egypt One site, shown in Fig. 9, clearly illustrates the main emissivity feature of silicate minerals (coarse quartz) at 8 to 9 μm and a smaller feature at 13 μm. The gaps in the spectrum are spectral regions not measured by the AIRS grating spectrometer. In contrast, the IASI interferometer is expected to make nearly continuous measurements across the infrared spectrum from about 4 μm to about 15 μm.

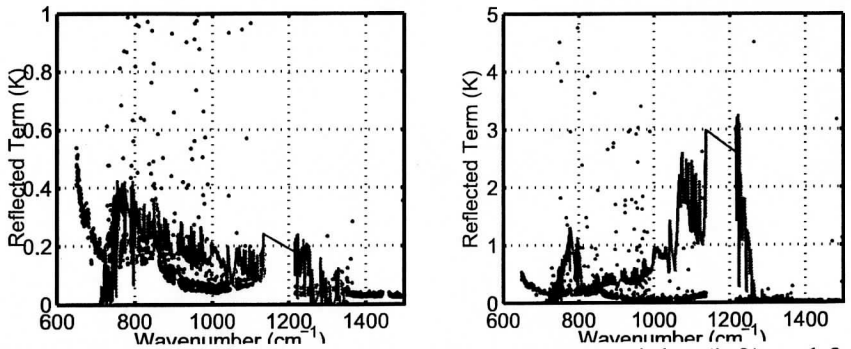

Figure 7. Reflected contribution (solid curve) for a 2% reflectivity (left) and for a quartz sand emissivity obtained from the JPL ASTER spectral library (right) compared to the AIRS noise estimate both for a 300 K scene.

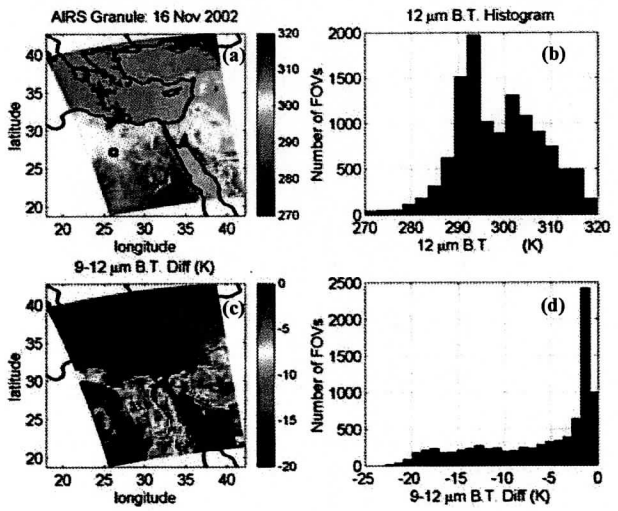

Figure 8. AIRS observations of (a) 12 μm brightness temperature at nominal 15-km resolution and (b) the corresponding brightness temperature histogram for a NASA Aqua overpass at 11:00-11:06 UTC on 16 November 2002. The difference between the AIRS 9 μm and 12 μm brightness temperature is shown in panel (c) and (d). Note that the 9

minus 12 μm observed brightness temperatures are close to zero for the water and vegetation scenes but can reach up to 20 degrees for scenes containing mostly exposed silicate minerals.

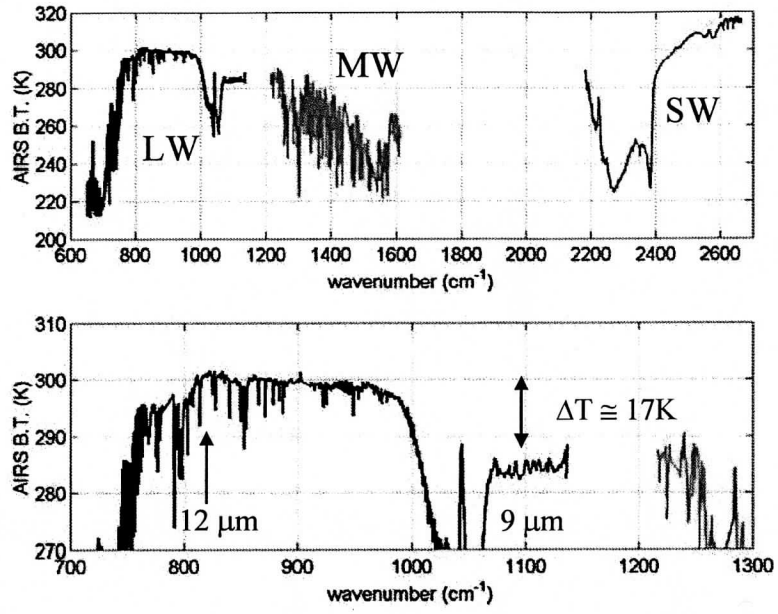

Figure 9. AIRS observed brightness temperature spectrum over the "Egypt One" validation site (identified by the square symbol in the previous figure) for a NASA Aqua daytime overpass at 11:03 UTC on 16 November 2002.

The analysis of the AIRS observations includes computation of 1) the raw relative emissivity, 2) the atmospheric corrected relative emissivity, and 3) the simultaneous solution of effective skin temperature and absolute emissivity. This approach is used to illustrate that the major surface emissivity spectral features are apparent even in the uncorrected AIRS observations, but that with the additional information provided by the ECMWF atmospheric model we can remove many of the effects of atmospheric contamination. Ultimately the atmospheric profile of temperature and water vapor will be obtained from the sounder data directly so that the use of NWP model data will be unnecessary. Finally the application of an online/offline technique is illustrated that can be used to simultaneously determine skin temperature and absolute infrared emissivity from individual AIRS fields of view.

The simplest analysis that does not require any additional information or calculations is the computation of a relative emissivity. Figure 10 shows a comparison of observations from the Egypt One desert site and from an ocean field of view in the Red Sea and the raw relative emissivity computed with T_{BT} equal to the mean observed brightness temperature in the 12 μm microwindow between 830 cm^{-1} and 832 cm^{-1} which is near a maximum in the quartz spectral emissivity known as the Christensen frequency. Note that an atmospheric correction has not yet been applied to these raw relative emissivity results. The strong spectral contrast due to the quartz mineral in the sand grains is apparent with a spectral contrast of about 25% (relative emissivity of 0.75) between 9 and

12 μm. Plotting the relative emissivity at 9 μm for all AIRS fields of view can be used to characterize the amount of bare soil/mineral contained in each AIRS footprint. Figure 10 shows the raw relative emissivity at 9 μm derived from the AIRS L1B observations as color-filled contour plots for both day-time and night-time granules. The same spatial information on the land surface emissivity is contained in the relative emissivity plots as in the brightness temperature differences, however the relative emissivity is normalized by the observed brightness temperature so it provides a more useful estimate of the infrared emission characteristics of the surface. One interesting feature to note is the indication that the Thessaly Plain in Greece has a strong 4 μm emissivity feature but does not have one at 9 μm, unlike the Sahara desert sands in which the 9 μm region has greater spectral contrast than at 4 μm. Figure 11 shows that for the indicated region, the 9 μm relative emissivities range between about 0.7 and 1 with the higher emissivities having more vegetation coverage.

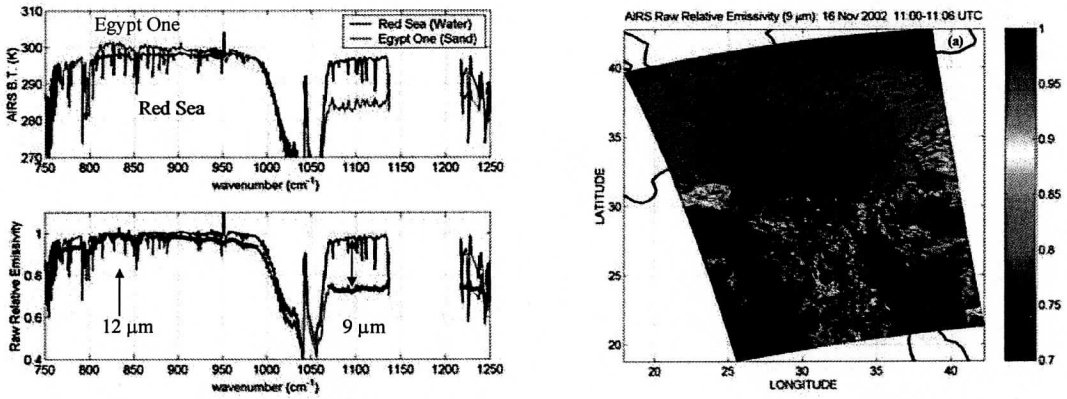

Figure 10. The upper panel shows a region of the AIRS observed brightness temperature spectrum for the Egypt One site (sand dunes) and for a field of view in the Red Sea (ocean water) for the same daytime overpass at 11:03 UTC on 16 November 2002. The lower panel shows the "raw" relative emissivity computed for the two scenes (without atmospheric correction). The black dots indicate the AIRS "microwindows" for which the raw relative emissivity approximation is valid.

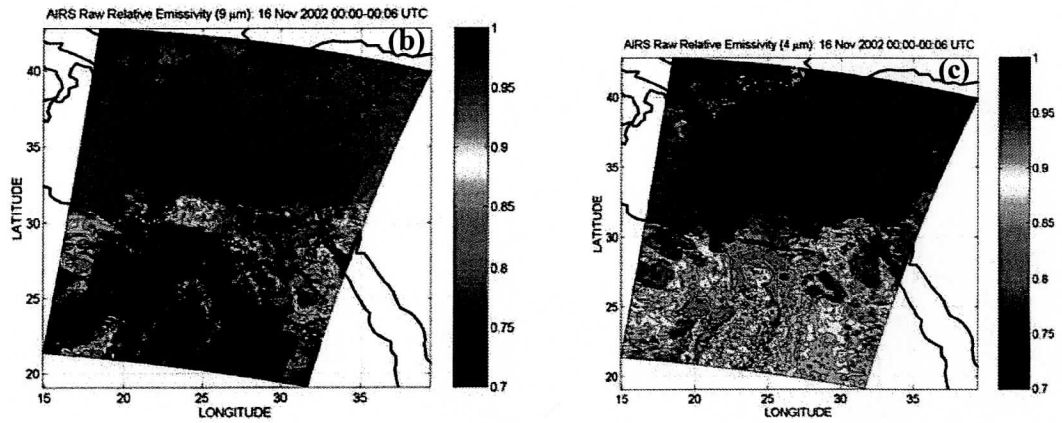

Figure 11. Raw relative emissivity shown as a contour map derived from the 15-km L1B AIRS radiances at (a) 9 μm during a daytime overpass and at (b) 9 μm and (c) 4 μm during a nightime overpass of the Aqua satellite on 16 November 2002. The observed brightness temperature at 12 μm is used as the reference temperature. At 9 μm the vegetated Nile river basin and the ocean coastal zones show up as high emissivity (>0.95) while the exposed desert sands have low emissivity (<0.8). The night-time measurements at 4 μm show less spectral contrast than 9 μm for most of the desert regions with the notable exception being a region in Greece where the relative emissivity at 4 μm is much lower than at 9 μm, perhaps indicating a smaller mineral grain size. In these maps, the cloud covered regions show up as black with emissivities greater than 1. The square symbol marks the location of the validation site in the Libyan Desert. Note that an atmospheric correction has not yet been applied to these results.

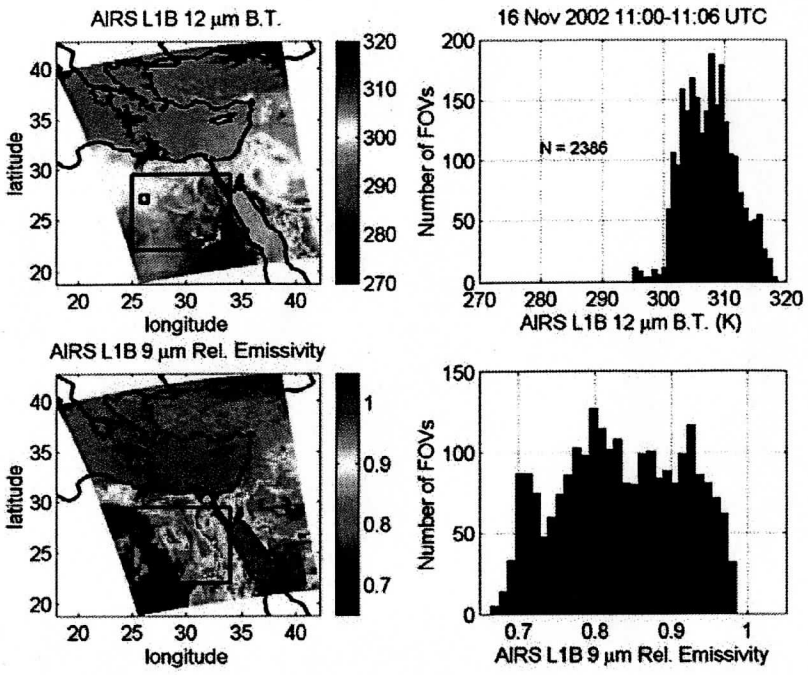

Figure 12. AIRS 12 μm brightness temperature map (upper left) for a six minute segment of AIRS data on 16 November 2002 11:00-11:06 UTC. The relative emissivity at 9 μm derived using Eq. 4 (lower left). The right-hand panels contain the histograms of the values within the large rectangular region. The square symbol marks the Egypt One validation site (27.12 N, 26.10 E) in the Libyan desert.

The next approach is to correct for the effect of atmospheric emission under the approximation that the thermal reflected term can be neglected. As shown in Figure 7, neglecting the thermal reflected term is not necessarily a good assumption over the desert where reflectivities can be quite high. However, for the purpose of illustration we have computed the atmospheric emission contribution using the ECMWF profile and a line-by-line model and computed an atmospherically corrected relative emissivity. Note that the normalization of the relative emissivity to unity at 12 μm requires that the skin temperature estimate be adjusted to account for the atmospheric transmission. This is illustrated in Figure 13 and 14 (left panel) which shows the skin temperature estimate prior to and after correction for atmospheric emission and transmission changes by just over 2 degrees. Most of the spectral line structure is removed by the atmospheric correction process but some residual noise and spectroscopic errors remain on absorption lines suggesting that only the micro-windows between absorption lines should be used in the derived relative emissivity estimate.

Finally the effect of including the thermal reflected term is illustrated in Figure 14 (right panel). Here only the microwindows are shown as dots, which avoids the noise introduced on the spectral lines. The comparison is with the spectral library quartz sand from the ASTER spectral library provided simply as an example. As described in Knuteson et al. (2004), the optimal skin temperature is determined by minimizing the

spectral variance on and off of atmospheric absorption lines in a selected wavenumber region. Note that the emissivity curve is now an absolute emissivity and the optimal skin temperature has increased by another 1.15 degrees Kelvin above the atmospherically corrected relative emissivity and a full 3.6 K above the 12 μm observed brightness temperature. Also note that the 9 μm emissivity has decreased below 0.7 suggesting that inclusion of the reflected thermal term leads to greater spectral contrast in this case.

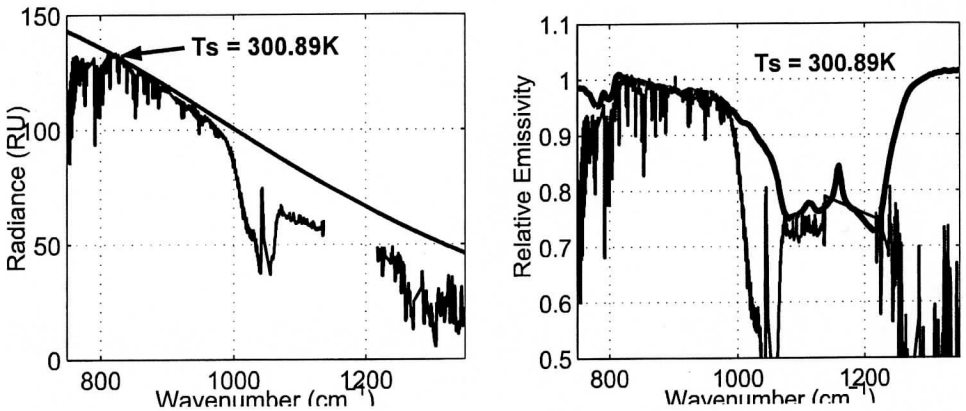

Figure 13. The AIRS radiance observation closest to the Egypt One validation site is shown (left) overlaid with a Planck radiance function for a temperature equal to the observed brightness temperature in the 12 μm region (830-832 cm^{-1}). The derived relative emissivity spectrum is shown in the right-hand panel compared to an example laboratory emissivity spectra obtained from the JPL ASTER library which has also been normalized to unity at 12 μm.

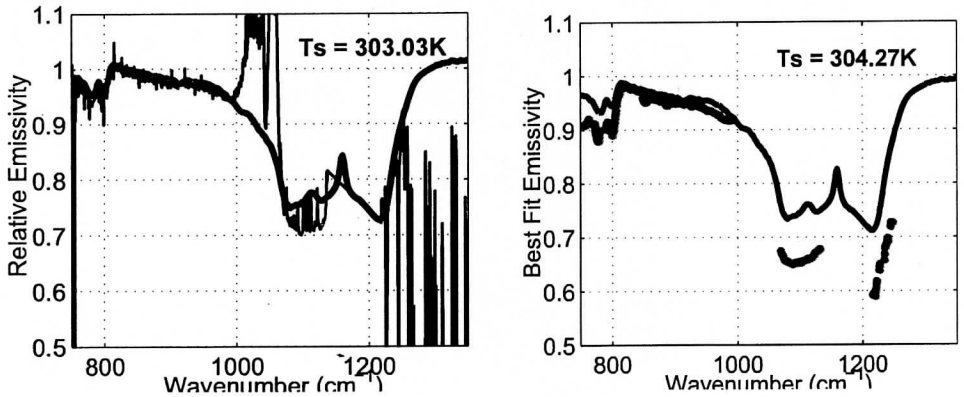

Figure 14. The left-hand panel shows the relative emissivity in Fig. B after correcting for atmospheric emission and transmission 3 compared with the quartz "alluvial" sand (solid line) from the ASTER spectral library. The right-hand panel shows the absolute value of the effective emissivity (symbols) obtained from Eq. 2 using the 970-980 cm^{-1} spectral region to determine the minimum spectral variance. Also shown are the skin temperature estimates obtained for each case.

In summary, an estimate of the spectral contrast in surface emissivity has been obtained with high spectral resolution over a satellite validation site in the Libyan Desert. The "Egypt One" site was chosen because it is a large, fairly uniform, sandy desert region suitable for evaluation of the 15-km footprints of the NASA AIRS advanced sounder. The results show a spectral contrast of more than 30% between 12 μm and 9 μm. The spectral contrast in the raw relative emissivity at 4 μm is also large (>10%) but less than that at 9 μm. These spectral features are generally consistent with laboratory emission spectra measured for coarse grains of the mineral quartz.

4.3 ARM Southern Great Plains Site

The ARM SGP site contains state of the art atmospheric and surface radiation measurements. This site is already being used in the validation of AIRS and MODIS atmospheric products so it is a natural choice for comparison of land surface products. As has been noted there have been several ground-based and aircraft campaigns in the vicinity of the ARM SGP site. Figure 15 shows the wheat growing belt of the central U.S. and the location of the ARM SGP site. The eastern portion of the SGP region is a permanent grassland used for ranching while the western portion is dominated by wheat growing. This wheat growing region has a strong seasonal variability in surface properties which are associated with the agricultural activity (tilling the soil, growth of winter wheat, and harvest in the early summer). The routine comparison of AIRS and MODIS retrievals at the ARM sites provides the best overall quality assessment of the science team algorithms for both surface and atmospheric products. Having atmospheric truth data along with the satellite observations provides a valuable validation component to the land surface emissivity remote sensing. This allows the algorithms for the direct retrieval of effective LST and LSE to be applied for multiple sensors. The measurement of surface emissivity data at these sites will extend the value of atmospheric data sets used in "training", "tuning", and "validation" of the satellite sounding products. In this manner, the results of the AIRS team products can be evaluated to verify improvements to the science team research algorithms.

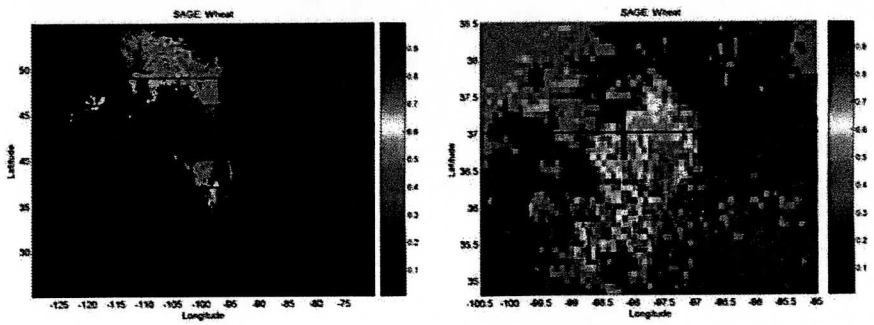

Figure 15. Land cover map of wheat belt (left) and DOE ARM SGP Site location (right).

The algorithm for the separation of land surface temperature and surface emissivity published in Knuteson et al. (2004) was applied to AIRS observations from a 16 November 2002 Aqua overpass at 19 UTC of the DOE ARM SGP site. The mean

observed high spectral resolution radiance used in the analysis is shown in Figure 16 in units of equivalent blackbody temperature compared to a line-by-line model calculation. The atmospheric transmission and emission are calculated using a line-by-line radiative transfer model (LBLRTM/HITRAN2000) and a coincident temperature and water vapor profile (Clough et al. 1992; Rothman et al. 1998). The atmospheric state profile was taken from a coincident ECMWF atmospheric state profile. The LBLRTM code was used to compute the total transmission between the surface and the sensor and the upwelling emission of the atmosphere above the surface (no surface or reflected terms). The total transmission and upwelling emission after reducing the spectral resolution to match the AIRS observations were also calculated along with the atmospheric downwelling emission at the surface. The standard deviation of the derived effective emissivity was computed over the spectral range [970 cm^{-1}, 980 cm^{-1}] for a range of effective surface temperatures. The "best fit" effective land surface emissivity was computed by substituting for the best fit surface temperature of 292.15 K. The left hand graph in Figure 17 illustrates the optimization process used to determine the "best fit" to the effective land surface temperature. The right hand graph in Figure 17 shows the raw land surface emissivity before noise spikes have been removed. The effective land surface emissivity derived from the mean AIRS observation and two extreme fields of view is compared in Figure 18 with a linear combination of pure scene types of vegetation and bare soil (measured by the authors using ground-based FTS at the ARM SGP site). The fact that the effective LSE derived can be approximated by a linear combination of two pure scene types is consistent with the definition of effective emissivity as a linear spatial weighting of the emissivity of pure scene types.

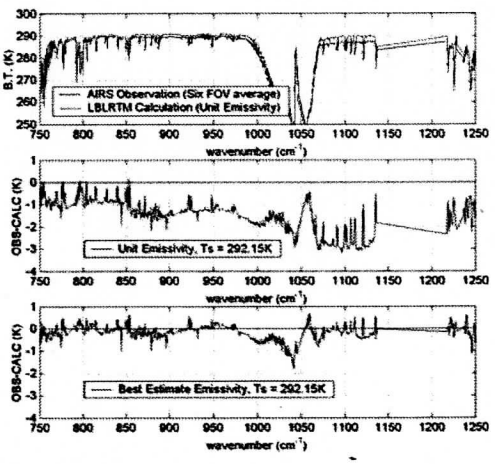

Figure 16. Mean of six observations from the NASA AIRS instrument near the SGP ARM central facility on 16 November 2002 (19 UTC overpass) compared to two line-by-line calculations. The calculations use the same atmospheric profile and surface skin temperature but make different assumptions about the surface emissivity. The error in the residual in the range 990-1070 cm^{-1} is caused by the use of a climatological ozone profile in the line-by-line calculations that does not match the observations perfectly. The gap between 1140 and 1220 cm^{-1} is a region that is not measured by the AIRS instrument. The use of the UW LSE model ("Best Estimate") is superior in accounting for the wavelength dependence of the infrared spectral residual compared to calculations that ignore the effect of land surface emissivity.

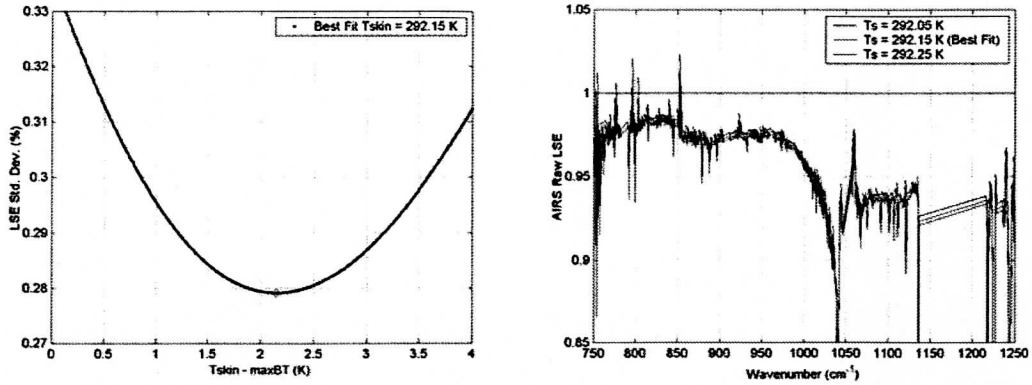

Figure 17. The left hand figure shows the minimization process used to determine the "best fit" effective land surface temperature for the selected AIRS observation. The right hand figure shows the raw surface emissivity derived using Eq. (11) and the "best fit" land surface temperature. Also shown is the derived emissivity for a surface temperature of plus and minus 0.1 K. The AIRS observations are from the 19 UTC overpass of north central Oklahoma on 16 Nov 2002. The investigator supplied temperature and emissivity separation algorithm that takes advantage of the unique advantages of high spectral resolution observations was used to create these results.

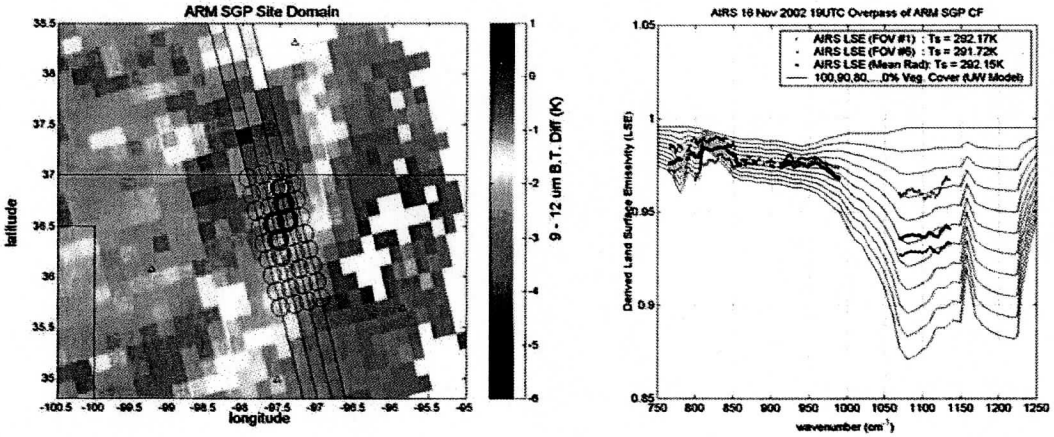

Figure 18. An image of surface emissivity at 15 km spatial resolution derived from AIRS observations over the DOE ARM SGP site is shown in the left hand panel. The right hand panel shows the AIRS effective surface emissivity for the colored circles shown in the left hand panel.

The launch of the NASA Aqua platform in 2002 with the EOS AIRS instrument opened a new era of high spectral resolution observations of infrared top of the atmosphere radiance in the thermal infrared. The UW LSE model for the ARM SGP site was developed in order to provide a "best estimate" of the surface emission in the vicinity of the ARM SGP central facility to complement the ARM atmospheric profile data. This "best estimate" of atmospheric and surface characteristics is being used in the validation of the AIRS level 1b and level 2 products over the ARM SGP site domain on a horizontal scale of about 50 km (Tobin et al. 2006). Figure 19 shows an example of the L1B

radiance "matchups" for one day (16 Nov 2002) illustrating the AIRS diurnal and spatial coverage. In Figure 20, the UW "prelaunch" estimate of vegetation fraction over ARM SGP is compared with vegetation fraction derived directly from the L1B radiance observations of AIRS a 20 month period (Nov 2002 – July 2004).

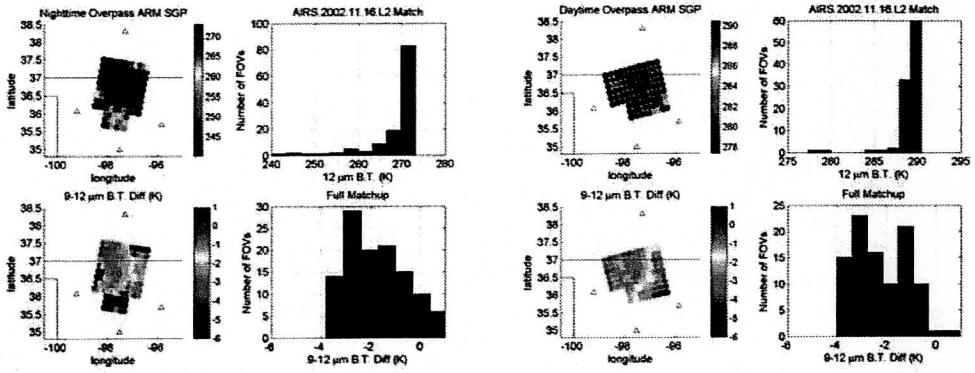

Figure 19. The infrared emissivity spectra in the vicinity of the DOE ARM SGP site is being modeled using a combination of measurements derived from ground-based, aircraft, and satellite high spectral resolution infrared observations. Note that land use patterns, i.e. pasture (East) and wheat farming (West) dominate the seasonal IR emissivity variations at this site. Retrospective model updates are expected.

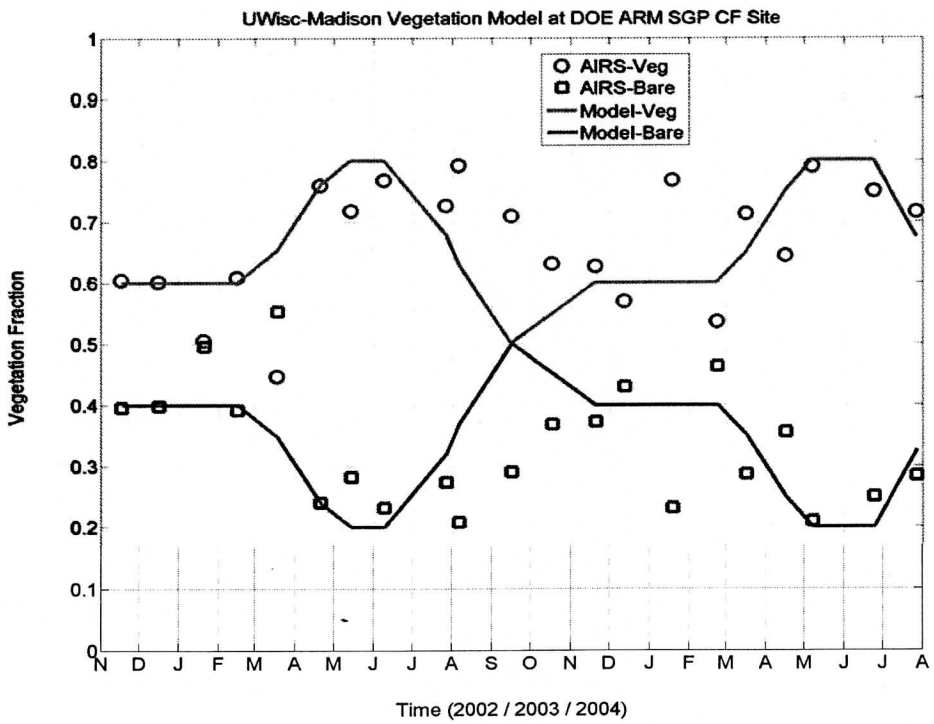

Figure 20. Vegetation fraction time series derived from AIRS infrared emissivity. The UW retrieved AIRS infrared emissivity spectra in the vicinity of the DOE ARM SGP site was used to fit a linear combination of bare soil and vegetated pure emissivity types (measured with UW groundbased FTS) yielding an effective vegetation fraction.

Conclusions of Southern Great Plains (SGP) analyses:

1. The absolute emissivity can be separated from the effective skin temperature for AIRS sounder fields of view using the method presented in Knuteson et al. (2004).

2. The AIRS absolute emissivity derived from the Knuteson et al. (2004) method was shown to be consistent with a linear combination of pure scene types based upon UW ground-based measurements.

3. A time series of AIRS observations at the ARM SGP site has been shown to capture the seasonal variations in the effective emissivity in this wheat growing region. The DOE ARM SGP site surface emissivity is important because of the use of this site for validation of retrieved atmospheric profiles of temperature and water vapor.

4.4 Global AIRS/MODIS Comparison

In this study the Level 3 gridded surface temperature and emissivity product derived from the Level 2 AIRS data is compared with MODIS Level 3 global products. The goal of this activity is to generate a time record of LST and LSE at a comparable spatial resolution. Since the AIRS L3 product is at 1 degree spatial resolution the MODIS data has been degraded from 5 km (0.05 degree) to 1 degree spatial resolution. The left panel of Figure 21 shows the overlap of the MODIS channels and AIRS channels that go into this analysis. The primary window channels which are at 12 μm, 11 μm, 8.5-9 μm, and 4 μm. Note that the 8.5μm MODIS channel does not overlap directly with the AIRS 9 μm channels but they both do sense the quartz doublet so are comparable with respect to bare soil emissivity. The right panel of Figure 21 is an example of the AIRS monthly skin temperature product which is determined for both ocean and land regions. Figure 22 shows the MODIS coverage of the 1 degree grid squares needed for comparison to AIRS L3 products. A cutoff is used on the MODIS LST fraction so that comparison to AIRS is only made when MODIS has sufficient clear sky data (> 50%) in a grid cell. Also shown in Figure 22 is an example of the MODIS minus AIRS skin temperature difference for the month of July 2003 showing good global coverage with the exception of tropical convective regions and high latitudes for with MODIS data is not available.

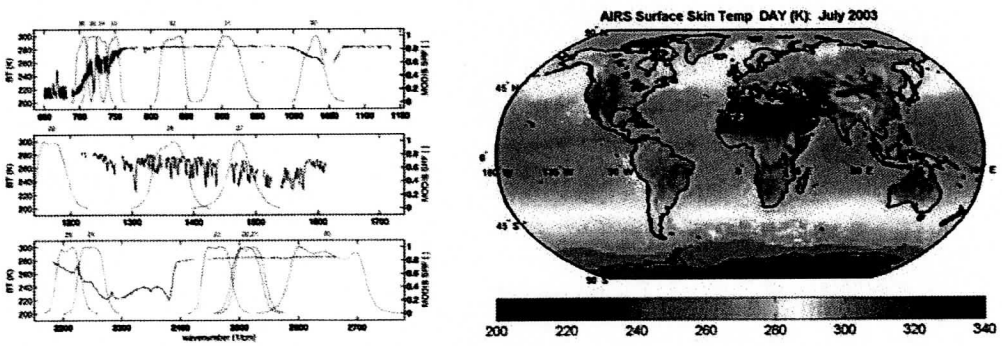

Figure 21. MODIS SRF overlaid on AIRS spectrum (left). Example global AIRS Tskin monthly product (right) for the month of July 2003 at 1 degree spatial resolution.

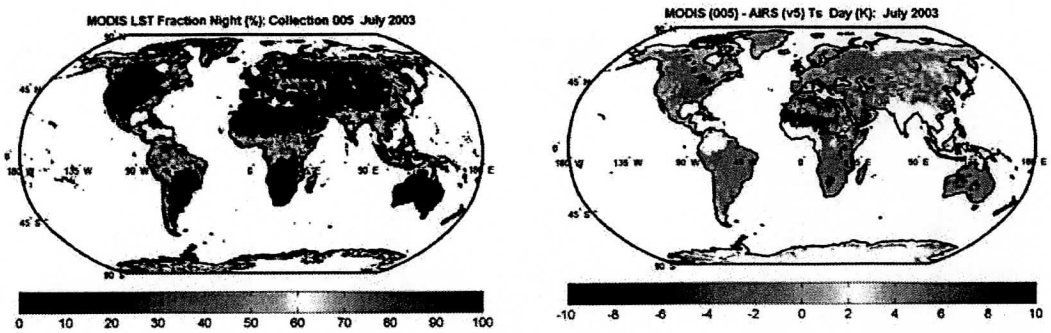

Figure 22. The percentage of MODIS Tskin values (at 5 km resolution) covering a 1 degree spatial grid cell is shown (left). Regions with low percentage coverage (<50%) are not included in the comparison with AIRS. The MODIS minus AIRS skin temperature difference is shown on the right panel for the month of July 2003.

The statistical analysis of the MODIS and AIRS Tskin comparison is complicated by the large variety of land cover types that comprise the Earth's land surface. Note for example the cold bias between MODIS and AIRS over desert regions shown in Figure 22. In order to usefully diagnose the MODIS minus AIRS Tskin differences we make use of the IGBP land type classification. Figure 23 shows a map of the 16 classes of the International Geosphere-Biosphere Project (IGBP) defined at 1 degree grid cell resolution.

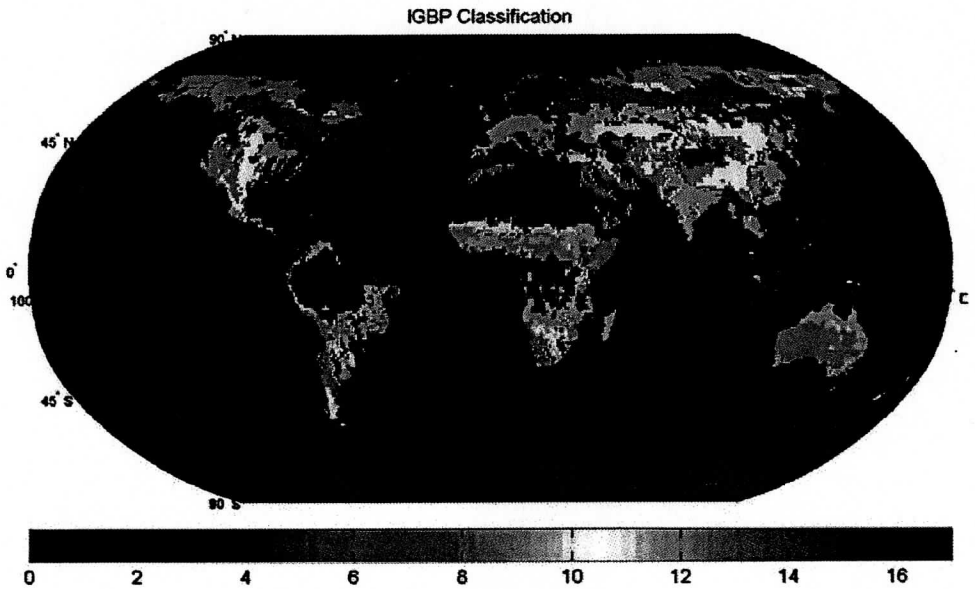

Figure 23. IGBP land classification at 1 degree spatial resolution.

A monthly time series of MODIS minus AIRS Tskin differences by land class is shown in Figure 24. The charts in Figure 24 are grouped by similar land types, i.e. forests, grassland/cropland, barren/savannah, and snow/ice. The upper four charts are a comparison with MODIS version 004 and the bottom set of four charts are with the

newer MODIS version 5. There is a significant degradation of results between MODIS version 4 and 5 suggesting a problem with the MODIS version 5 product algorithm. This is summarized in terms of skin temperature in Figure 25 which shows the mean and standard deviation for each land type for the MODIS version 4 and version 5 comparison to the same AIRS collection 5 data.

Comparison of clear sky MODIS and cloud cleared AIRS skin temperaure over cold snow/ice covered surfaces (mainly in the polar regions) is complicated by the use of the MODIS cloud mask in the identification of the clear MODIS footprints used in the comparison. A similar problem occurs for AIRS because uniform clouds can be flagged as clear sky and then can be averaged into the monthly L3 product leading to large biases in skin temperature for the monthly average. Additional work is required in the analysis of this polar dataset. Detection of clouds over snow/ice remain a problem for both AIRS and MODIS as seen in Figures 24 and 25 for the snow/ice land types which show seasonal errors of up to 4 degrees. Excluding snow/ice, the nighttime v004 agreement is excellent.

The effect of skin temperature biases is also seen in the emissivity comparison shown in Figures 26 and 27 where it appears that cutoffs in the MODIS version 5 emissivity at 12 and 11 μm are introducing biases in both skin temperature and in the derived emissivity at 8.5 μm and presumably also at 4 μm. This analysis shows in a comprehensive manner that MODIS version 4 is in better agreement with AIRS collection 5 than the newer MODIS version 5. Since these results were presented at the NCDC LST workshop in April 2008, the MODIS land team has moved quickly to version 6 which should repair the bias introduced in version 5 (Knuteson et al. 2008). Also the MODIS version 004 product has been continued forward in time as the current preferred baseline MODIS product. The work supported under this grant was influential in quickly identifying this algorithm problem and communicating the information to the appropriate science teams. This example of comparison of AIRS and MODIS supports the original assertion that routine comparison of sounder and imager products provides an excellent tool in the validation of future climate products on operational satellite sensors.

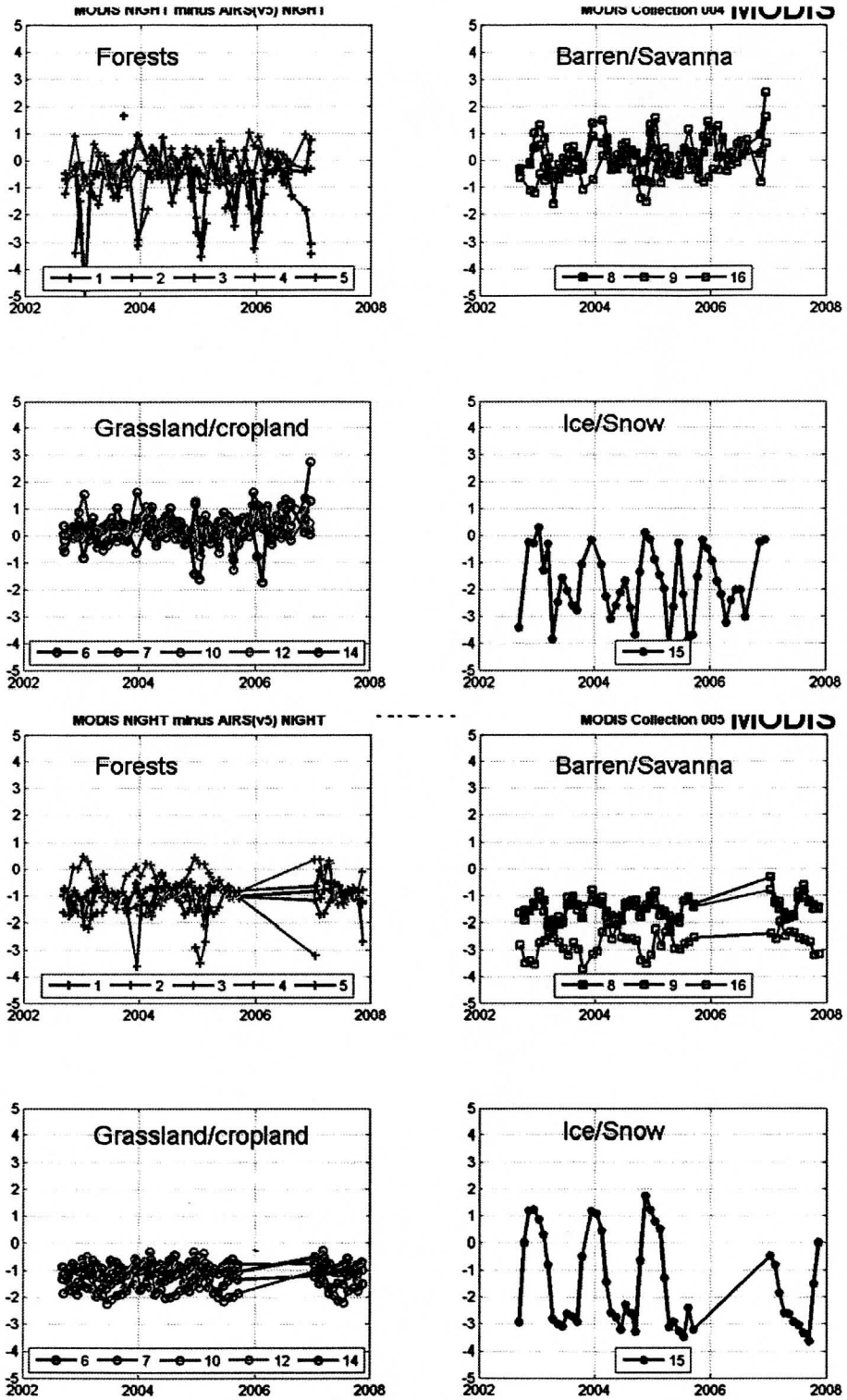

Figure 24. Nighttime MODIS minus AIRS skin temperature difference by IGBP class. Top four panels are against MODIS v4 and lower four panels are versus MODIS v5. The MODIS v4 results agree better with AIRS than the MODIS v5 product.

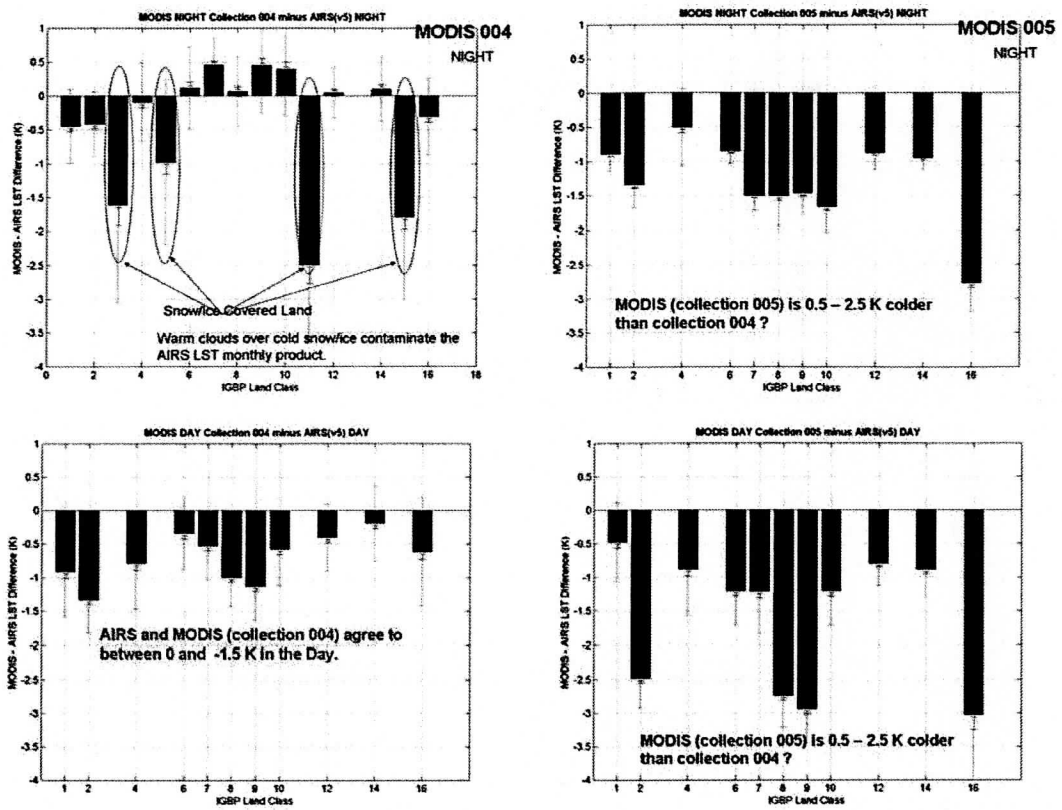

Figure 25. Comparison of MODIS minus AIRS Tskin for both MODIS v004 and v005.

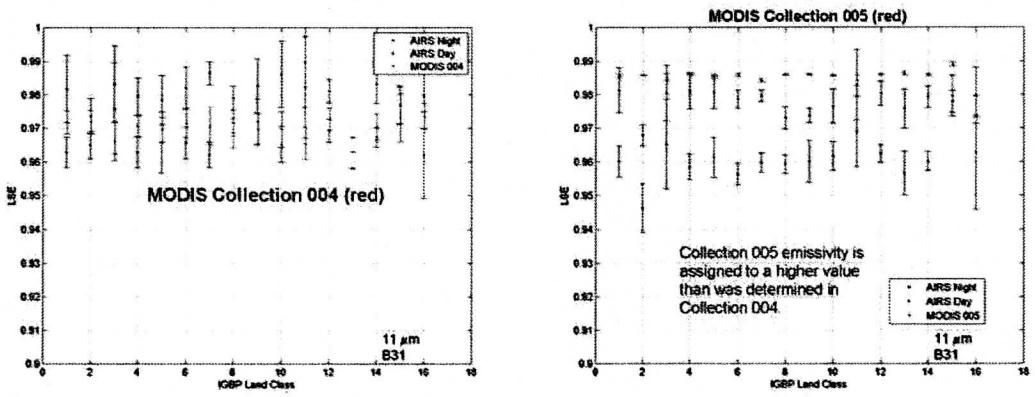

Figure 26. Comparison of MODIS minus AIRS 11 μm emissivity for both MODIS v004 and v005 over a five year record 2003 to 2007. There is a strong relationship between the 11 μm emissivity value and the derived skin temperature. The MODIS v004 emissivity lies between the AIRS day and night emissivity and excluding snow/ice classes the agreement in Tskin is between 0.5 and 1.5 K for all land classes which is quite good for a global comparison. The MODIS v005 emissivity at 11 μm has clearly been "set" to a very narrow range of values which are higher than those found in MODIS v004. This causes the derived skin temperature to be too cold relative to AIRS which causes the MODIS minus AIRS Tskin difference for v005 to be biased negative.

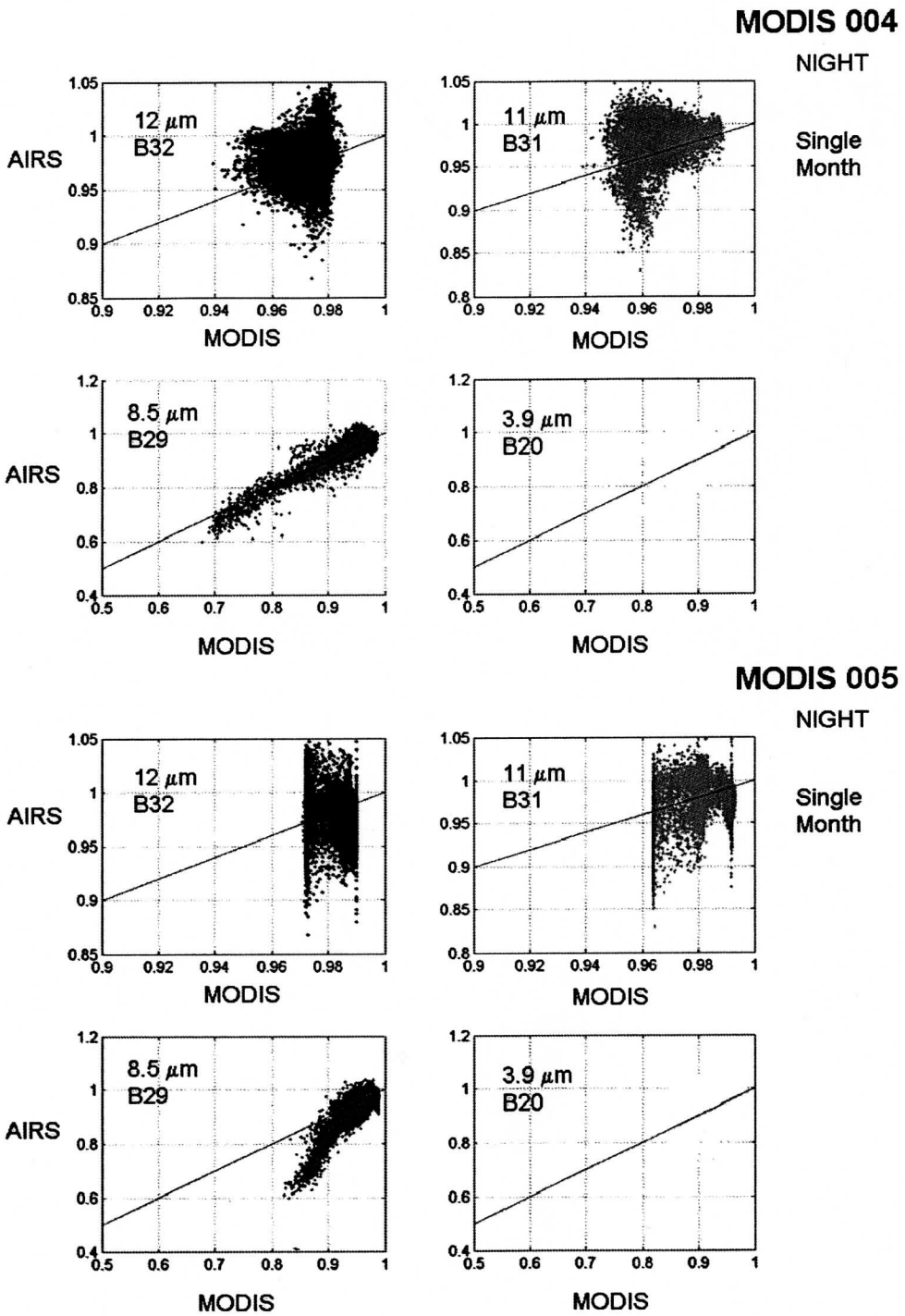

Figure 27. A comparison for the month of July 2003 between the AIRS and MODIS emissivities at four wavelengths (12 μm, 11 μm, 8.5 μm, and 3.9 μm). Note in particular the good correlation over barren soils seen in the MODIS v004 comparison with AIRS at 8.5 μm (the quartz signature). This agreement is seriously degraded in the MODIS v005 comparison. Also note the cutoffs used in the MODIS v005 emissivity at 12 and 11 μm. Clearly the MODIS v004 is more consistent with the AIRS retrieval results.

5. Summary of Accomplishments and Future Work

This report addresses the following two important goals, (1) better utilization of satellite sounding data over land and (2) study of the evolution of land surface characteristics. The report is intended to assist in the interpretation of the spatial and temporal variation of EOS land surface temperature and emissivity measurements and in the quantification of the relation of these measurements to natural and human forced environmental changes. This work has contributed directly to improving the predictive capabilities of weather and climate models by providing confidence in the land products of two key EOS sensors; MODIS and AIRS which are being used to develop climatologies of surface properties at NWP centers. Although it is outside the scope of this report, it is worth noting that the key EOS Aqua sensor measurements will be continued with the VIIRS and CrIS sensors during the following NPP and NPOESS programs. The following results where obtained during this study:

- ***The algorithm for the separation of land surface effective emissivity and skin temperature presented in Knuteson et al (2004) has been successfully applied*** to extreme desert conditions for which conventional methods are problematic.

- A time series of AIRS observations at the DOE Southern Great Plains site has demonstrated ***the ability of AIRS to detect seasonal changes*** in land surface emissivity, which is directly related to human land use patterns.

- Global comparison of the MODIS v4 Clear Day/Night algorithm and AIRS v5 cloud-cleared multi-channel regression retrieval agree to within 0.5 K at night (excluding snow/ice covered land) and between 0 and -1.5 K during the Day. ***There is excellent agreement between AIRS and MODIS skin temperature and this agreement is also true for the IR emissivities derived from each sensor.***

- ***A problem was identified in the recent MODIS collection 005 Clear Land Classification algorithm.*** It is 0.5 to 3 degrees colder than collection 004 (and also colder than AIRS v5). The change in assumed MODIS emissivity is consistent with this LST change. This raises a question about land cover classification schemes and how to avoid building in systematic biases. These results were presented at the NCDC LST workshop in April 2008 and are leading to the acceleration of MODIS collection 006 which should avoid the problems encountered in collection 005.

- The simple fact that biases can be assessed through a comparison of AIRS and MODIS suggests that a ***continuous comparison of imager and sounder LST products will be a useful quality check on future operational algorithms***. This is the primary lessons learned in this project and it completely consistent with the concept of using multiple data streams as cross-checks to create a valid satellite climatology of land products.

6. References

Aumann, H. H., T. S. Pagano, L. Strow, 2001: Atmospheric Infrared Sounder (AIRS) on the Earth Observing System, *Proc. SPIE* 4151, 115–125, Hyperspectral Remote Sensing of the Land and Atmosphere, William L. Smith and Yoshifumi Yasuoka (Eds.), 2001.

Balba A.M., 1980: Desertification in North Africa. *Transactions of the 12th International Congress of Soil Science Symposia* papers III, 914–935.

Bower, Nicholas, Robert O. Knuteson, and Hank E. Revercomb, 1999: High spectral resolution land surface temperature and emissivity measurement in the thermal infrared. Preprints, *10th Conference on Atmospheric Radiation: A Symposium with tributes to the works of Verner E. Suomi*, Madison, WI, 28 June–2 July 1999. American Meteorological Society, Boston, MA.

Chedin, A., M. A. Scott, C. Wahiche, and P. Moulinier, 1985: The improved initialization inversion method: a high resolution physical method for temperature retrievals from the TIROS-N series. *J. Climate Appl. Meteor.*, 24, 124-143.

Chahine, M. T., H. Aumann, M. Goldberg, L. McMillin, P. Rosenkranz, D. Staelin, L. Strow, J. Susskind, 1999: AIRS Algorithm Theoretical Basis Document, AIRS-Team Retrieval for Core Products and Geophysical Parameters, Level 2, JPL D-17006, Version 2.0, December 15, 1999.

Clough, S. A., M. J. Iacono, and J.-L. Moncet, 1992: Line-by-line calculation of atmospheric fluxes and cooling rates: Application to water vapor, *J. Geophys. Res.*, 97, 15761–15785, 1992.

Derber, J. C., and W.-S. Wu, 1998: The use of TOVS cloud-cleared radiances in the NCEP SSI analysis system. *Mon. Wea.Rev.*, 126, 2287 - 2299.

DeSlover, D. H., R. O. Knuteson, B. J. Osborne, D. K. Zhou, and W. L. Smith, 2002: Validation of aircraft-measured land surface emissivity, *SPIE's Third International Asia-Pacific Symposium on Remote Sensing of the Atmosphere, Environment, and Space*, Hangzhou, China, 23-27 October 2002. SPIE, Bellingham, WA.

Diebel, D., M. Langevin, D. Klaes, P. Courtier, T. Phulpin, F. Cayla, G. Chalon, 1997: The advanced atmospheric temperature sounder IASI, *Proc. EUMETSAT User Conference*.

Dozier, J. and Z. Wan, 1994: Development of practical multiband algorithms for estimating land-surface temperature from EOS/MODIS Data, *Adv. Space Res.*, 14, (3)81-(3)90.

Hodges, J. C. F., Friedl, M. A., and Strahler, A. H., 2001: The MODIS Global Land Cover Product: New data sets for global land surface parameterization, *Proc. Global Change Open Science Conference*, Amsterdam.

Korb, A. R., J. W. Salisbury, and D. D'Aria, 1994: Thermal-infrared remote sensing and Kirchoff's law 2. Laboratory measurements. *J. Geophys. Res.*, 104(B7), 15339-15350.

Korb, A. R., P. Dybwad, W. Wadsworth, and J. W. Salisbury, 1996: Portable Fourier transform infrared spectroradiometer for field measurement of radiance and emissivity, *Applied Optics*, 35, 1679-1692.

Knuteson R. O. et al., 2008: Comparison of NASA AIRS and MODIS Land Surface Temperature and Infrared Emissivity Measurements from the EOS AQUA platform, presentation at the International Workshop on the Retrieval and Use of Land Surface Temperature: Bridging the Gaps, NCDC, Asheville, NC, April 2008.

Knuteson, R. O., F. A. Best, D. H. Deslover, B. J. Osborne, H. E. Revercomb, W. L. Smith, Sr., 2004: Infrared land surface remote sensing using high spectral resolution aircraft observations, *Adv. Space Res.*, Volume 33, Issue 7, 2004, pp 1114-1119

Knuteson, R. O., R. G. Dedecker, W. F. Feltz, B. J. Osborne, H. E. Revercomb, and D. C. Tobin, 2003: Infrared land surface emissivity in the vicinity of the ARM SGP Central Facility, in *Proc. 13th ARM Science Team Meeting*, Broomfield, CO, March 31 – April 4, 2003.

Knuteson, R. O., D. H. Deslover, A. M. Larar, B. J. Osborne, H. E. Revercomb, J. F. Short, W. L. Smith, and R. Tanamachi, 2002: Infrared land surface remote sensing using high spectral resolution observations, *SPIE 3rd International Asia-Pacific Environmental Remote Sensing Symposium* 2002, Remote Sensing of the Atmosphere, Ocean, Environment, and Space, Hangzhou, China, 23-27 October 2002. SPIE, Bellingham, WA.

Knuteson, R., B. Osborne, J. Short, H. Revercomb, D. Tobin, S. Nasiri , 2001a: Progress towards a characterization of the infrared emissivity of the land surface in the vicinity of the ARM SGP Central Facility: Surface (S-AERI) and airborne sensors (NAST-I / S-HIS), *Proc. 11th ARM Science Team Meeting*, Atlanta, GA, March 19-23, 2001.

Knuteson, R. O., B. J. Osborne, H. E. Revercomb, D. C. Tobin, and W. L. Smith, 2001b: Infrared land surface emissivity retrieval from high-spectral resolution upwelling radiance. In *11th Conference on Satellite Meteorology and Oceanography*, Madison, WI, 15–18 October 2001, American Meteorological Society, Boston, MA, 688-691.

Li, J., W. P. Menzel, Z. Yang, R. A. Frey, and S. A Ackerman, 2003: High spatial resolution surface and cloud type classification from MODIS multi-spectral band measurements. J. Appl. Meteor., Vol.42, No.2.

Li, J., J. P. Nelson III, T. Schmit, W. P. Menzel, C. C. Schmidt, and H.-L. Huang, 1998: Retrieval of total atmospheric ozone from GOES sounder radiance measurements with high spatial and temporal resolution. Preprints, *1st Intl. Asia-Pacific Symposium on Remote Sensing of the Atmosphere, Environment, and Space*, Beijing, China, Intl. Soc. Opt. Engineering.

Ma, X. L., Z. M. Wan, C. C. Moeller, W. P. Menzel, and L. E. Gumley, 2002: Simultaneous retrieval of atmospheric profiles, land-surface temperature, and surface emissivity from Moderate-Resolution Imaging Spectroradiometer thermal infrared data: extension of a two-step physical algorithm, Appl. Opt., 41, pp. 909 - 924.

Ma, X. L., Z. M. Wan, C. C. Moeller, W. P. Menzel, L. E. Gumley, and Y.L. Zhang, 2000: Retrieval of geophysical parameters from Moderate Resolution Imaging Spectroradiometer thermal infrared data: evaluation of a two-step physical algorithm, Appl. Opt., 39, pp. 3537 - 3550.

Moeller C. C., D. D. LaPorte, W. P. Menzel, and H. E. Revercomb, 2001: Evaluation of MODIS emissive band radiometric performance using MAS data collected during

TX-2001, *11th Conference on Satellite Meteorology and Oceanography Meeting*, AMS.

Moriyama, M. and K. Arai, 1994: An inversion for emissivity-temperature separation with ASTER data, *Adv. Space Res.*, 14, (3)57-(3)70.

Murphy, R. E., R. L. Taylor, S. P. Neeck, B. A. Wielicki, B. R. Barkstrom, M. Crison, J. R. Swenson, 1998: NPOESS preparatory project (NPP), *Proc.* SPIE, 3498, 72-75, Sensors, Systems, and Next-Generation Satellites II, Hiroyuki Fujisada (Ed.), 1998.

Nelson, C. S., J. D. Cunningham, The National Polar-Orbiting Operational Environmental Satellite System future U.S. Environmental Observing System, *6th Symposium on Integrated Observing Systems*, Orlando, FL, AMS.

Osborne, B. J., R. O. Knuteson, H. E. Revercomb, J. F. Short, and D. C. Tobin, 2003: Ground truth measurements for validation of AIRS land surface temperature and emissivity products at the Southern Great Plains validation site, in *Fourier Transform Spectroscopy*, OSA Technical Digest (Optical Society of America, Washington DC, 2003), Quebec City, 3–6 February 2003.

Revercomb, H. E., D. C. Tobin, R. O. Knuteson, F. A. Best, W. L. Smith, P. van Delst, D. D. LaPorte, S. D. Ellingson, M. W. Werner, R. G. Dedecker, R. K. Garcia, N. Ciganovich, and H. B. Howell, 2003: Atmospheric Infrared Sounder (AIRS) validation with Scanning-HIS, in *Fourier Transform Spectroscopy*, OSA Technical Digest (Optical Society of America, Washington DC, 2003), Quebec City, 3–6 February 2003.

Revercomb, H. E., V. P. Walden, D. C. Tobin, J. Anderson, F. A. Best, N. C. Ciganovich, R. G. Dedecker, T. Dirkx, S. C. Ellington, R. K. Garcia, R. Herbsleb, R. O. Knuteson, D. LaPorte, D. McRae, and M. Werner, 1998: Recent results from two new aircraft-based Fourier transform interferometers: The Scanning High-resolution Interferometer Sounder and the NPOESS Atmospheric Sounder Testbed Interferometer, *8th International Workshop on Atmospheric Science from Space using Fourier Transform Spectrometry*, Toulouse, France, 1998.

Running, W. W., C. O. Justice, V. Salomonson, D. Hall, J. Barker, Y. J. Kaufman, A. H. Srahler, A. R. Heute, J. P. Muller, V. Vanderbilt, Z. M. Wan, P. Teillet, and D. Carneggie, 1994: Terrestrial remote sensing science and algorithms planned for EOS/MODIS. *Int. J. Rem. Sens.*, 15(17), 3587-3620.

Rothman, L. S., et al., 1998: The HITRAN molecular spectroscopic database and HAWKS: 1996 Edition, *J. Quant. Spectros. Radiat. Transfer*, 60, 665-710.

Salisbury, J. W., and D. M. D'Aria, 1992: Emissivity of terrestrial materials in the 8-14 μm atmospheric window: *Remote Sens. Environ.*, 42, 83-106.

Salisbury, J. W., and D. M. D'Aria, 1994: Emissivity of terrestrial materials in the 3-5 μm atmospheric window, *Remote Sens. Environ.*, 47, 345-361.

Schmit T. J., W. F. Feltz, W. P. Menzel, J. Jung, A. P. Noel, J. N. Heil, J. P. Nelson III, G. S. Wade, 2002: Validation and use of GOES sounder moisture information. *Wea. Forecasting*, 17, 139-154.

Stokes, G. M. and S. E. Schwartz, 1994: The Atmospheric Radiation Measurement (ARM) Program: Programmatic background and design of the Cloud and Radiation TestBed. *Bull. Amer. Meteor. Soc.*, 75, 1201-1221.

Strahler, A., J. Townshend, D. Muchoney, J. Borak, M. Friedl, S. Gopal, A. Hyman, A. Moody, and E. Lambin, 1996: MODIS Land Cover and Land-Cover Change Algorithm Theoretical Basis Document (ATBD), Version 4.1.

Smith, W.L., 1989: Satellite soundings—current status and future prospects. *Adv. Space Res.*, 9(7), 363-372.

Susskind, J., Rosenfield, J., Reuter, D., and Chanhine, M. T. (1984). Remote sensing of weather and climate parameters from HIRS2/MSU on TIROS-N. *J. Geophys. Res.*, 89(D3), 4677-4697.

Susskind, J., C. Barnet, and J. Blaisdell, 1998: Determination of atmospheric and surface parameters from simulated AIRS/AMSU/HSB sounding data: Retrieval and cloud clearing methodology, *Adv. Space Res.*, 21, 369–384.

Tanamachi, R., R. Knuteson, V. Walden, 2001: Data quality control and preliminary data analysis from the Interferometric Monitor for Greenhouse gases (IMG) data set, *11th Conference on Satellite Meteorology and Oceanography*, Madison, WI, 14-18 October 2001, American Meteorological Society, Boston, MA, 2001.

Tobin, D., H. Revercomb, W. Feltz, R. Knuteson, D. Turner, B. Lesht, L. Strow, C. Barnet, E. Fetzer, 2003: ARM site atmospheric state best estimates for AIRS validation, in *Proc. 13th ARM Science Team Meeting*, Broomfield, CO, March 31–April 4, 2003.

Tobin, D. C, H. E. Revercomb, and D. D. Turner, 2002: Overview of the AMR/FIRE Water Vapor Experiment (AFWEX), in *Proc. 12th ARM Science Team Meeting*, St. Petersburg, FL, 8-12 March 2002.

Tobin, D. C., H. E. Revercomb, R. O. Knuteson, B. M. Lesht, L. L. Strow, S. E. Hannon, W. F. Feltz, L. A. Moy, E. J. Fetzer, and T. S. Cress (2006), Atmospheric Radiation Measurement site atmospheric state best estimates for Atmospheric Infrared Sounder temperature and water vapor retrieval validation, J. Geophys. Res., 111, D09S14, doi:10.1029/2005JD006103.

Wan, Z. and Dozier, J., 1997: A physics-based algorithm for retrieving land-surface emissivity and temperature from EOS/MODIS data. *IEEE. Trans. Geosci. Remote Sens.*, 35, 980-996.

Wan, Z., 1999: MODIS land-surface temperature Algorithm Theoretical Basis Document (LST ATBD). Technical Report Version 3.3, Institute for Computational Earth System Science, University of California, Santa Barbara.

Xie, Rongrong, 1994: Retrieving surface temperature and emissivity from high spectral resolution radiance observations. M.S. thesis, Dept. of Atmospheric and Oceanic Sciences, University of Wisconsin-Madison, xi, 105p.